

# Flat photonic surface bands pinned between Dirac points

Dario Jukić,<sup>1,2,\*</sup> Hrvoje Buljan,<sup>1</sup> Dung-Hai Lee,<sup>3</sup> John D. Joannopoulos,<sup>2</sup> and Marin Soljačić<sup>2</sup>

<sup>1</sup>Department of Physics, University of Zagreb, Bijenička c. 32, Zagreb 10000, Croatia

<sup>2</sup>Research Laboratory of Electronics, Massachusetts Institute of Technology, 77 Massachusetts Avenue, Cambridge, Massachusetts 02139, USA

<sup>3</sup>Department of Physics, University of California at Berkeley, 366 LeConte Hall MC 7300, Berkeley, California 94720, USA

\*Corresponding author: djukic@phy.hr

Received October 26, 2012; accepted November 27, 2012;

posted December 3, 2012 (Doc. ID 178698); published December 14, 2012

We point out that 2D photonic crystals (PhCs) can support surface bands that are pinned to Dirac points. These bands can be made very flat by optimizing the parameters of the system. Surface modes are found at the interface of two different cladding materials: one is a PhC with Dirac linear dispersion for the TE mode, and the other is a PhC that has a broad TE gap at the Dirac frequency. © 2012 Optical Society of America

OCIS codes: 050.5298, 230.5298, 240.6690.

Photonic crystals (PhCs) have been studied extensively due to their importance in theory, experiments, and applications [1–3]. It has been shown that light dispersion in certain 2D PhCs can possess Dirac points [4–9]. Dirac points are characterized by conical (i.e., linear) dispersion and can be found in PhCs with triangular lattice symmetry [4–7,9]. Linear and nonlinear honeycomb photonic lattices (where the wave dynamics obeys a nonlinear Schrödinger-like equation) and pertinent phenomena such as conical diffraction have also been studied [10]. In part these studies have been motivated by experimental realization of graphene: a monolayer of carbon atoms arranged in honeycomb lattice with Dirac dispersion and extremely interesting properties [11–13]. Along with the bulk dispersion properties, real photonic systems are characterized by surface (edge) states at the boundaries. Because of their versatility, PhCs are especially suitable for the studies of these localized modes [3]. Among surface states, flat surface bands are also important in the context of slow light dispersion and for achieving large density of states. We note here that dispersion-free surface states in graphene-like photonic lattices have been observed recently [14]. In this Letter we show that, in 2D PhCs, it is possible to design surface bands that are pinned to Dirac points. Furthermore, we show that the dispersion characteristics can be tailored: by varying the parameters of the system, a specific band pinned between Dirac points can be made extremely flat. To the best of our knowledge, this is the first study of flat surface bands in the Dirac pseudogap region in the context of PhCs.

We start by introducing a 2D triangular lattice of dielectric rods with a high dielectric index  $\epsilon_h$  embedded in a low-index material  $\epsilon_l$ . As has been shown in [4–7,9], this structure can be tailored to have Dirac points for TE modes. We tune the system parameters so that the lattice has a large Dirac pseudogap: we want the Dirac point to be sufficiently separated from other TE bands and conical dispersion to extend throughout this region. We choose the high dielectric constant of the rods to be  $\epsilon_h = 12$  and their radius  $r_1 = 0.31a$  ( $a$  is the lattice constant). For the low-index material, we take  $\epsilon_l = 1$ . The structure is shown in the inset of Fig. 1(a). Our calculations are performed using the frequency-domain method for solving Maxwell equations in periodic systems [15].

In Fig. 1(a) we plot the TE projected band structure (PBS) of our triangular lattice. As a projection axis we take one particular direction of the primitive cell (parallel to the horizontal edge of the structure in the inset). We denote it as  $\parallel$  axis and  $k_{\parallel}$  as its projection of the 2D wave vector. The dispersion  $\omega(k_{\parallel})$  depicts presence of two Dirac points,  $k_D = \pm 1/3(2\pi/a)$ , in the first Brillouin zone of the PBS, centered at frequency  $\omega_D \approx 0.45(2\pi c/a)$ . The linear dispersion encompasses states in the second and the third TE projected band. In addition, Fig. 1(b) shows the surface plot of the 2D band structure for the second and the third TE band. We clearly see the characteristic graphene-like hexagonal pattern of Dirac points with conical dispersion around the central frequency.

At this point, in order to introduce surface states into our 2D system, we need to modify the geometry. As a first step, we cut the triangular lattice of rods along the  $\parallel$  axis, thus creating a semi-infinite structure. We show that, under certain conditions, we can find surface states at its edges. Namely, since the Dirac point is above the light line, we have to ensure that these surface states will not couple to the outer regions. That is, we need to attach another photonic structure as a cladding material: this cladding should have a TE bandgap in the Dirac pseudogap region. We find that a properly chosen triangular lattice of low dielectric holes can satisfy this criterion. In particular, we use holes with dielectric constant  $\epsilon_l$  and radius  $r_2 = 0.48a$ , embedded in a high dielectric region with  $\epsilon_h$ .

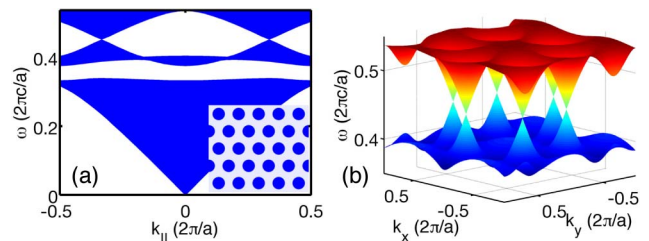


Fig. 1. (Color online) (a) TE PBS of 2D photonic graphene-like system. Dirac points are found between the second and the third TE photonic band. The inset depicts triangular structure of high- $\epsilon$  ( $\epsilon_h = 12$ ) rods in low- $\epsilon$  ( $\epsilon_l = 1$ ) media, with  $r_1/a = 0.31$ . (b) Surface plot of the 2D TE band structure (second and third band) with the characteristic hexagonal pattern: Dirac points with conical dispersion.

Therefore, the final construct involves an interface geometry between two different 2D PhCs: the semi-infinite triangular lattice of rods (*lower cladding*) and the semi-infinite triangular lattice of holes (*upper cladding*). Since the translational symmetry in the perpendicular direction is broken, we write  $k_{\parallel} \equiv k$ . Next we introduce the termination parameter  $t$  to define the particular realization of the cladding interface as follows. We keep positions of the rods and the holes in two semi-infinite structures fixed such that the centers of all the rods and all the holes lie on the same lattice. We choose to have one line of boundary cells divided into two parts along the  $k$  axis. The termination parameter  $t$  ( $0 \leq t \leq 1$ ) measures the extent to which the boundary cell is occupied by the lower cladding material. Particular examples of dielectric structure for various  $t$ 's are plotted in the insets on the right of the Fig. 2 (translucent green).

Figure 2 shows surface bands in the Dirac pseudogap region. In general, surface states originate from the bulk, and as  $t$  changes they move within the pseudogap region: the net effect of changing  $t$  from 0 to 1 is to move one bulk band from the upper (third) to the lower (second) TE band. Here we demonstrate that (i) surface bands can be pinned to Dirac points and (ii) for some  $t$  we may find one or even two (top and bottom) surface bands. Results for three different values of termination parameter  $t$  are presented:  $t = 0.55$  (red solid),  $t = 0.6$  (black dot-dashed), and  $t = 0.8$  (magenta dashed). Blue and green areas present bulk modes of two independent claddings. For  $t = 0.55$  and  $t = 0.6$  we have two surface bands (top and bottom) at each  $t$ . Bottom bands are pinned to two Dirac points, and our calculations show that this statement is also valid for smaller values of  $t$  (not shown). That is, if the *entire* Dirac pseudogap region between left and right Dirac points can support a surface band (for all, or some, values of  $t$ ), the band is pinned since the bandgap at Dirac points is zero.

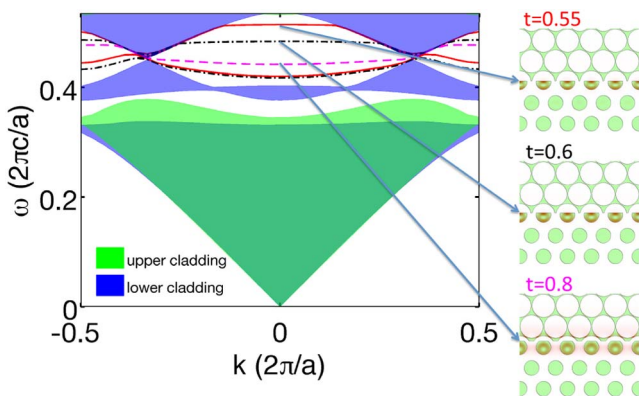


Fig. 2. (Color online) Surface bands within the Dirac pseudogap. We plot results with termination parameter  $t$  (see text for details) for three particular junctures of the two cladding materials:  $t = 0.55$  (red solid),  $t = 0.6$  (black dot-dashed), and  $t = 0.8$  (magenta dashed). PBSs of bulk of two cladding PhCs are shown for both lower cladding (blue) and upper cladding (green) material. In the insets on the right we plot the electric-field energy density of three states (at  $k = 0$ ) from the top surface bands (up to bottom:  $t = 0.55$ ,  $t = 0.6$ , and  $t = 0.8$ ). Energy density is in red color, superimposed on the high dielectric pattern (translucent green).

However, at  $t = 0.55$  and  $t = 0.6$ , an additional (top) surface band is present: it is pulled from the upper bulk region. We see that, since this surface band has just left the bulk region, it does not initially extend between the left and the right Dirac points. By increasing  $t$ , this top band approaches the central (Dirac) frequency and becomes pinned between the two Dirac points as well. This can be nicely seen for  $t = 0.8$ . Moreover, for  $t = 0.8$ , no bottom band is present since, for this value of  $t$ , the bottom band has already entered the lower bulk region. Finally, in order to illustrate the localized character of the surface modes, in the insets on the right we plot the electric-field energy density (in red color) for three different values of  $t$  (at  $k = 0$ ), superimposed on their dielectric structures.

Now we proceed to an important finding of this Letter: our system allows for construction of a superflat surface band. We emphasize the following: the facts that the bands are pinned and that their curvature (second derivative at  $k = 0$ ) must alter sign when changing  $t$  from 0 to 1 guarantee that we can expect to find flat bands for some parameter values. However, we can do even more by carefully optimizing different parameters in our structure. For this we utilize a nonlinear (and derivative-free) optimization algorithm [16,17] in order to minimize the width of the surface band in the region around  $k = 0$  [specifically, between  $k = -1/4(2\pi/a)$  and  $k = 1/4(2\pi/a)$ ]. In the present numerical calculations we have chosen to vary the termination  $t$ , radius of the rods  $r_1$ , and radius of the holes  $r_2$ . By changing these three parameters we indeed find a very flat band pinned between Dirac points. This surface band structure is plotted (top red curve) in Fig. 3 for the optimized values of  $t = 0.66$ ,  $r_1/a \approx 0.306$ , and  $r_2/a \approx 0.480$ . The flat region extends from the left to the right Dirac point, thus occupying most of the 1D Brillouin zone. In addition, we also note that another surface band (bottom red curve) in the pseudogap region is present for these parameters. Blue and green areas represent bulk modes of the two constituent claddings, as in Fig. 2. A short comment is needed to explain the small gap that seemingly opens at the Dirac points: this is a result of the finite size of our system in

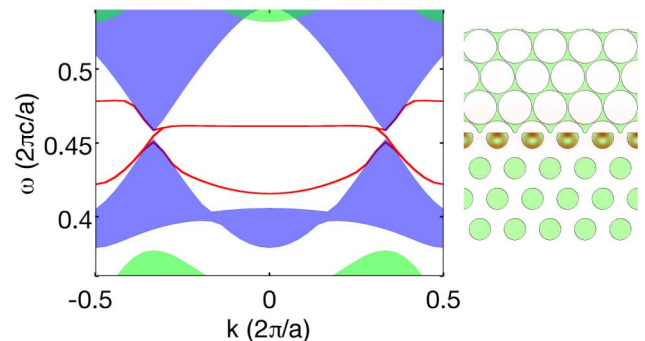


Fig. 3. (Color online) Superflat dispersion of the surface band between two Dirac points (top red curve). Here  $t = 0.66$ ,  $r_1/a \approx 0.306$ , and  $r_2/a \approx 0.480$ . An additional (bottom) surface band is also present. Blue and green areas are PBSs of two independent claddings, as in Fig. 2. In the inset on the right we plot the electric-field energy density of the flat surface mode (at  $k = 0$ ).

numerical simulations. For the sake of completeness, in the inset on the right we depict the electric-field energy density of the superflat surface mode (at  $k = 0$ ).

Finally, we comment on the analogy between the surface states in PhCs and in graphene. In the case of the electronic structure of graphene, the nonzero winding number and the chiral symmetry of the Dirac Hamiltonian ensure that there is a *zero-energy* flat band between two Dirac points along the zigzag edge [18–20]. However, we emphasize here that, in PhCs with triangular (honeycomb) symmetry, one cannot guarantee to have *exactly* flat bands [8]. This point requires careful treatment in future studies of these analogies. In particular, it has been shown recently that the effective Hamiltonian (for triangular PhCs) close to Dirac point can be mapped into the Dirac Hamiltonian [21].

In summary, we have constructed TE surface bands in a 2D PhC system that are pinned to Dirac points in reciprocal space. Our system consists of two cladding materials: the first is a 2D PhC that exhibits linear (Dirac) dispersion between the second and the third TE band, and the second PhC has a bandgap in the region where the first PhC has the Dirac-cone dispersion. This interface can support one or even two different surface modes, depending on the particular realization of the system. We have shown, by optimizing the parameters of our system, that superflat surface bands can exist in the Dirac pseudogap region. We expect that this Letter will inspire study of surface bands with large density of states in PhCs with conical dispersion.

D. J., M. S., and J. D. J. were supported in part by the U.S. Army Research Office under contract W911NF-07-D-0004. D. J. and H. B. acknowledge support by the Croatian Ministry of Science, grant no. 119-0000000-1015.

## References

1. S. John, Phys. Rev. Lett. **58**, 2486 (1987).
2. E. Yablonovitch, Phys. Rev. Lett. **58**, 2059 (1987).

3. J. D. Joannopoulos, S. G. Johnson, J. N. Winn, and R. D. Meade, *Photonic Crystals: Molding the Flow of Light* (Princeton University, 2008).
4. M. Plihal and A. A. Maradudin, Phys. Rev. B **44**, 8565 (1991).
5. R. A. Sepkhanov, Ya. B. Bazaliy, and C. W. J. Beenakker, Phys. Rev. A **75**, 063813 (2007).
6. F. D. M. Haldane and S. Raghu, Phys. Rev. Lett. **100**, 013904 (2008).
7. S. Raghu and F. D. M. Haldane, Phys. Rev. A **78**, 033834 (2008).
8. T. Ochiai and M. Onoda, Phys. Rev. B **80**, 155103 (2009).
9. S. R. Zandbergen and M. J. A. de Dood, Phys. Rev. Lett. **104**, 043903 (2010).
10. O. Peleg, G. Bartal, B. Freedman, O. Manela, M. Segev, and D. Christodoulides, Phys. Rev. Lett. **98**, 103901 (2007).
11. K. S. Novoselov, A. K. Geim, S. V. Morozov, D. Jiang, Y. Zhang, S. V. Dubonos, I. V. Grigorieva, and A. A. Firsov, Science **306**, 666 (2004).
12. A. K. Geim and K. S. Novoselov, Nat. Mater. **6**, 183 (2007).
13. A. H. C. Neto, F. Guinea, N. M. R. Peres, K. S. Novoselov, and A. K. Geim, Rev. Mod. Phys. **81**, 109 (2009).
14. Y. Plotnik, M. C. Rechtsman, D. Song, M. Heinrich, A. Szameit, N. Malkova, Z. Chen, and M. Segev, in *CLEO: QELS-Fundamental Science*, OSA Technical Digest (Optical Society of America, 2012), paper QF2H.6.
15. S. G. Johnson and J. D. Joannopoulos, Opt. Express **8**, 173 (2001).
16. S. G. Johnson, The NLOpt nonlinear-optimization package, <http://ab-initio.mit.edu/nlopt>.
17. M. J. D. Powell, in *Proceedings of the 40th Workshop on Large Scale Nonlinear Optimization* (Springer, 2006), pp. 255–297.
18. K. Nakada, M. Fujita, G. Dresselhaus, and M. S. Dresselhaus, Phys. Rev. B **54**, 17954 (1996).
19. S. Ryu and Y. Hatsugai, Phys. Rev. Lett. **89**, 077002 (2002).
20. R. S. K. Mong and V. Shivamoggi, Phys. Rev. B **83**, 125109 (2011).
21. J. Mei, Y. Wu, C. T. Chan, and Z.-Q. Zhang, Phys. Rev. B **86**, 035141 (2012).